Moroccan Journal of Chemistry
ISSN : 2351-812X

Mor. J. Chem., 2023, Volume 11, Issue 3, Page 818-830
https://revues.imist.ma/index.php/morjchem
https://doi.org/10.48317/IMIST.PRSM/morjchem-v11i3.40773

Crystal structure, Hirshfeld surface analysis and computational studies of (E)-2,2-dimethyl-4-styryl-2,3-dihydro-1H-benzo[b][1,4]diazepine

Odame F. [1] *, Madanhire T.[2], Hosten E. C.[2], Lobb K.[3],

[1]*Department of Basic Sciences, University of Health and Allied Sciences, PMB 31, Ho, Ghana*
[2]*Department of Chemistry, Nelson Mandela University, P.O. Box 77000, Gqeberha 6031, South Africa*
[3]*Department of Chemistry, Rhodes University, P.O. Box 94, Makhanda 6140, South Africa*

**Corresponding author, Email address: felixessah15@gmail.com*

Received *12 June 2023,*
Revised *04 July 2023,*
Accepted *07 July 2023*

Citation*: Odame F., Madanhire T., Hosten E. C., Lobb K (2023) Crystal structure, Hirshfeld surface analysis and computational studies of (E)-2,2-dimethyl-4-styryl-2,3-dihydro-1H-benzo [b][1,4]diazepine, Mor. J. Chem., 14(3), 818-830.*

Abstract: The crystal structure, Hirshfeld surface analysis, and computational studies of (*E*)-2,2-dimethyl-4-styryl-2,3-dihydro-1H-benzo[b][1,4]diazepine have been presented. The compound crystallized in the monoclinic space group *P21/c* with 8 molecules in its unit cell. A comparison of the experimental and computed bond lengths and bond angles showed good agreement among the results with varying deviations from each other. A discussion of the Hirshfeld surface analysis of the compound have been carried out to provide insight into the structural properties of the compound.

Keywords: Benzodiazepine, Hirshfeld surface analysis, monoclinic, computational studies

1. Introduction

Some chloropyrazine conjugated benzothiazepines have been synthesized and characterized using different spectroscopic methods. The compounds were tested for their anti-tubercular and cytotoxic activities. The compounds showed some activity against the human normal liver cell line LO_2 (Shaik, *et al* 2021). Some thiazole containing oxazepine derivatives have been synthesized by the action of a catalyst and by microwave irradiation, the compounds were characterized by spectroscopy (Taha, 2017). A variety of benzodiazepine derivatives have been accessed by the reaction of 4-methyl *o*-phenylenediamine with 4-amino acetophenone using ammonium chloride as catalyst under microwave irradiation. The synthesized compounds showed high activity against *Escherichia coli* and *Bacillus puimilus* (Rasheed *et al*, 2021).

Some triazolo-benzodiazepines have been studied for their pi-pi interactions. *In-silico* ADMET evaluations of the compounds showed more than 96% intestinal absorption for all compounds. The *in-silico* ADMET results showed that the molecules could be used as therapeutic agents in the treatment of depression (Belhassan *et al*, 2019; Tabti *et al*, 2022; Koubi *et al*, 2022; Kositsyn *et al*, 2023). Two quinolone derivatives have been synthesized and their structures elucidated using single crystal X-ray diffraction techniques. The compounds crystallized in the *P21/n* (monoclinic) space group with four

independent molecules in the asymmetric unit cell (Bano *et al*, 2017). The synthesis of a series of 1,3,4,5-tetrahydro-2H-1,5-benzodiazepines has been achieved by the reaction of DHA (dehydroacetic acid), *o*-PDA (*o*-phenylenediamine) and aromatic aldehydes in the presence of a catalytic amount of TFA (trifluoroacetic acid). The compounds were crystallized and their structures were determined using single-crystal X-ray diffractometry, and evaluated for their *in-vitro* cytotoxic effects (Faidallah *et al*, 2015). The solid-state geometric and conformational parameters of the X-ray structures of some benzodiazepine derivatives have been analyzed. DFT quantum mechanical calculations were used to study the electronic features of the different substituents. The conformations of the molecules with optimized geometry were analyzed and the relative charge distribution around the benzodiazepine ring and electrostatic potential maps on the electronic density surfaces were obtained (Gomes *et al*, 2011). We herein report, the crystal structure, Hirshfeld surface analysis and computational studies of (*E*)-2,2-dimethyl-4-styryl-2,3-dihydro-1H-benzo[b][1,4]diazepine derivative. A discussion on the single crystal XRD data of (*E*)-2,2-dimethyl-4-styryl-2,3-dihydro-1H-benzo[b][1,4] diazepine, has been presented to provide insights into the structural properties of the compound. The computed and experimental bond lengths, bond angles, vibrational frequencies, ^{1}H NMR as well as the Hirshfeld surface analysis of the compound has been discussed.

2. Methodology

2.1 Materials and Physical measurements

Analytical grade reagents and solvents for synthesis such as *o*-phenylenediamine, 2-chlorobenzaldehyde, and 4-methylpent-3-en-2-one were obtained from Sigma Aldrich (USA) whilst ethanol, acetone and methanol were obtained from Merck Chemicals (SA). The chemicals were used as received (i.e. without further purification). The reaction was followed with TLC using ethyl acetate: petroleum ether (1:1). ^{1}H NMR and ^{13}C NMR spectra were recorded on a Bruker Avance AV 400 MHz spectrometer operating at 400 MHz for ^{1}H and 100 MHz for ^{13}C. FT–IR spectra were recorded on a Bruker Platinum ATR Spectrophotometer Tensor 27. Microanalysis was performed using a Vario Elementar Microcube ELIII. Melting points were obtained using a Stuart Lasec SMP30. The masses were determined using a PerkinElmer GC Clarus 580 Gas Chromatograph interfaced with a Mass Spectrometer PerkinElmer (Clarus SQ 8 S).

2.2 Synthesis of (E)-2,2-dimethyl-4-styryl-2,3-dihydro-1H-benzo[b][1,4]diazepine

Benzaldehyde (0.01 mol, 1.06 g) was added to 2,2,4-trimethyl-2,3-dihydro-1H-benzo[b][1,4] diazepine (0.01 mol, 1.883 g) in methanol and heated under reflux for 8 h. The reaction mixture was transferred into a beaker and allowed to stand overnight in the fume hood. The product was recrystallized and obtained as a yellow solid from ethanol:acetone (1:1) Yield = 74 %, (2.04 g) Mp = 132−133 °C. ^{1}H NMR (ppm): 7.69 (d, J = 7.2 Hz, 2H), 7.40 (t, J = 7.2 Hz, 2H), 7.36 (s, 1H), 7.12 (s, 1H), 7.06 (m, 1H), 6.95 (m, 1H), 8.87 (m, 2H), 4.95 (s, 1H), 2.55 (s, 2H), 1.30 (s, 6H). ^{13}C NMR (ppm): 168.0 (C=N), 139.8 (C), 136.5 (CH), 132.4 (CH), 129.4 (CH), 128.6 (CH), 127.8 (CH), 126.3 (CH), 121.5 (CH), 120.5 (CH), 67.2 (C), 40.2 (CH_2), 30.6 (CH_3). IR (ν_{max}, cm^{-1}): 3053 (N–H), 3022 (C-H), 2924 (C-H), 1627 (C=N), 1576 (C=C), 1560 (C=C), 1456 (C–N). Anal. calcd. for $C_{19}H_{20}N_2$: C, 82.57; H, 7.29; N, 10.14. Found for $C_{19}H_{20}N_2$: C, 82.53; H, 7.24; N, 10.10. Found: 276. 25. LRMS (*m/z*, M^+): Expected mass = 276.38.

2.*3 X-ray crystallographic Determination*

X-ray diffraction analysis of the compound was performed at 296 K using a Bruker Kappa Apex II diffractometer with monochromated Mo Kα radiation (λ = 0.71073 A). The data collection was done

using APEX II (APEX2, 2010) whilst SAINT (APEX2, 2010) was used for cell refinement and data reduction. The structure was solved by direct methods using SHELXS–2018 (Sheldrick, 2008), and refined by least-squares procedures using SHELXL-2013 (Hubschle *et al*, 2011), with SHELXLE as a graphical interface. All non-hydrogen atoms were refined anisotropically. Carbon-bound H atoms were placed in calculated positions (C–H 0.95 Å for aromatic carbon atoms and C–H 0.99 Å for methylene groups) and were included in the refinement in the riding model approximation, with Uiso (H) set to 1.2Ueq (C). The H atoms of the methyl groups were allowed to rotate with a fixed angle around the C–C bond to best fit the experimental electron density (HFIX 137 in the SHELX program suite (APEX2, 2010), with Uiso (H) set to 1.5Ueq (C). Nitrogen-bound H atoms were located on a difference Fourier map and refined freely. Data were corrected for absorption effects using the numerical method implemented in SADABS (APEX2, 2010).

2.4 Computational studies

The calculations were carried out using Gaussian 09 program. The structures were fully optimized in the gas phase in the singlet ground state at the density functional theory (DFT) using the WB97XD/(6-31G+(p,d), WB97XD/(lanl2dz), B3PW91/(6-31G+(p,d) and B3PW91/(lanl2dz) functionals and basis set. During the preliminary work 11 functionals and basis set were used and compared with the literature. (Safna Hussan *et al*, 2019, Sevvanthi, *et al*, 2020, Bronisz, *et al*, 2006, Sarala, *et al*, 2021, El Ghayati *et al*, 2021). The functionals and basis set that gave values most consistent with the experimental values were reported in this work. The optimized structures corresponded to a minimum. The results were viewed in Avogadro or Gaussview 6.0. Gaussian 09 was used to compute the vibrational frequencies (IR), and ^{1}H NMR of the compounds

2.5 Justification for using lanl2dz basis set

In the computational studies the use of lanl2dz basis set has been limited to the computation of metal complexes, but it has also been used for the computation of sulphur-containing compounds (Elangovan *et al*, 2011, Flores-Hidalgo *et al*, 2011, Selvaraju *et al*, 2015). The choice of lanl2dz as a basis set was based the results of the preliminary work with the compound.

3. Results and Discussion

3.1 Chemistry

The compound was recrystallized from ethanol:acetone (1:1) as yellow crystals. The crystallographic data, selected bond lengths and bond angles for the crystal structure of (*E*)-2,2-dimethyl-4-styryl-2,3-dihydro-1H-benzo[b][1,4]diazepine are provided in **Tables 1** and **2.** The ORTEP diagram is presented in **Figure 1**. The compound had an apparent orthorhombic symmetry but true monoclinic symmetry because the crystals were pseudo-merohedrally twinned (Hamdane, *et al* 2009). It was crystallized in the monoclinic space group *P21/c.* The bond distances N21-C21, N21-C21 and N21-C26 which were 1.264(2), 1.400(2) and 1.290(1) Å are consistent with carbonyls, whilst the bond distances of C21-C22, C21-C27 and C22-C23 which are 1.509(1), 1.493(1) and 1.536(2) Å are typical of C-C single bonds (Odame *et al*, 2021; Ait Lahcen *et al*, 2023; Odame *et al*, 2021; El Assyry *et al*, 2013; Odame *et al*, 2013).

The bond angles of C21-N21-C211, C26-N21-C211 and C23-N22-C212 which are 119.8(4), 122.2(2) and 123.9(1)° respectively. Whilst the bond angles of N21-C21-C22, N21-C21-C27 and N22-C23-C22 are 123.3(1), 111.6(1) and 108.2(1)°.

Table 1 Crystallographic data and structure refinement summary for compound **1**

Property	Compound 1
Formula	$C_{19}H_{20}N_2$
CCDC	2141380
Formula Weight	276.37
Crystal System	Monoclinic
Space group	*P21/c*
a [Å]	9.5081(16)
b [Å]	19.067(3)
c [Å]	17.878(3)
α [°]	90
B [°]	90.007(8)
γ [°]	90
V [Å^3]	3241.1(9)
Z	8
D(calc) [g/cm^3]	1.133
Mu(MoKa) [/mm]	0.067
F(000)	1184
Crystal Size [mm]	0.13 x 0.33 x 0.50
Temperature (K)	296
Radiation [Å]	0.71073
MoKa	
Theta Min-Max [°]	2.1, 28.3
Dataset	-12: 10 ; -25: 19 ; -23: 23
Tot., Uniq. Data, R(int)	43774, 7943, 0.034
Observed Data [I > 2.0 sigma(I)]	4552
Nref,	7943
Npar	443
R	0.0479
$_wR_2$	0.1282
S	1.02
Min. Resd. Dens. [e/Å^3]	-0.18
Max. Resd. Dens. [e/Å^3]	0.22

3.2 Comparison of theoretical and experimental bond parameters

A summary of theoretical and experimental bond lengths and bond angles for the compound using WB97XD/(6-31G+(p,d), WB97XD/(lanl2dz), B3PW91/(6-31G+(p,d) and B3PW91/(lanl2dz) functionals and basis sets is provided in **Table 2**. The bond length of C21-C22 was experimentally determined as 1.509(1) Å, whilst the computed bond length gave deviations between 0.003 and 0.005 Å from the experimental values. For the amide bonds N21-C21, N21-C211, N22-C23 and N22-C212 the experimental bond lengths obtained were 1.260(2), 1.400(2), 1.472(2) and 1.394(2) Å, respectively, the computed values deviated by 0.001 and 0.051 Å. The bond lengths of C21-C27, C22-C23 and C23-C25 were experimentally determined as 1.493(1), 1.536(2) and 1.524(2) Å whilst the computed values gave deviations between 0.003 and 0.021 Å. The bond lengths of C23-C24, C26-C29 and C28-C221 were experimentally determined as 1.524(2), 1.560(5) and 1.486(3) Å with deviations between 0.003 and 0.033 Å representing the lowest and largest deviations, respectively, from the experimental values. The bond angles of C21-N21-C211, C23-N22-C212 and N21-C21-C22 were experimentally determined as 119.8(4), 123.9(1) and 123.3(1),° whilst the computed values gave deviations of between 0.6 and 10.8° from the experimental values. The bond angles of N21-C21-C27, N22-C23-C25 and N22-C23-C24 were experimentally determined as 111.6(1), 106.9(1) and 110.4(1)° with deviations between 0.4 and 3.2° for the computed values. The bond angles of C11-N11-C111 and C13-N12-C112 were experimentally determined as 120.3(1) and 121.1(1)° with deviations between 1.4 and 10.3° representing the lowest and largest deviations, respectively, from the experimental values.

Table 2 Summary of theoretical and experimental bond lengths (Å), and bond angles (°) for (*E*)-2,2-dimethyl-4-styryl-2,3-dihydro-*1H*-benzo[b][1,4]diazepine using WB97XD/ (6-31G+(p,d), WB97XD/(lanl2dz), B3PW91/(6-31G+(p,d) and B3PW91/(lanl2dz) functionals and basis set.

Bond length (Å)							
Compound 1							
Experimental		WB97XD/ (6-31G +(p.d)	WB97XD/(lanl2dz)	B3PW91/ (6-31G+(p.d)	B3PW91/ (lanl2dz)	Minimum Deviation	Maximum Deviation
N21-C21	1.260(2)	1.286	1.301	1.295	1.311	0.026	0.051
N21-C211	1.400(2)	1.399	1.414	1.389	1.404	0.001	0.014
N22-C23	1.472(2)	1.464	1.464	1.459	1.468	0.004	0.013
N22-C212	1.394(2)	1.390	1.389	1.381	1.388	0.004	0.013
C21-C22	1.509(1)	1.512	1.512	1.509	1.514	0.003	0.005
C21-C27	1.493(1)	1.474	1.473	1.463	1.464	0.019	0.03
C22-C23	1.536(2)	1.533	1.557	1.542	1.557	0.003	0.021
N11-C11	1.294(2)	1.286	1.301	1.295	1.311	0.001	0.017
N11-C111	1.406(2)	1.399	1.414	1.389	1.404	0.002	0.008
N12-C112	1.405(2)	1.390	1.389	1.381	1.388	0.015	0.024
C23-C25	1.524(2)	1.532	1.541	1.533	1.542	0.008	0.018
N12-C13	1.474(2)	1.464	1.464	1.459	1.468	0.006	0.015
C23-C24	1.524(2)	1.537	1.557	1.537	1.546	0.013	0.033
C26-C29	1.560(5)	1.533	1.558	1.542	1.557	0.003	0.027
C28-C221	1.486(3)	1.472	1.476	1.463	1.468	0.010	0.023
Bond angles (°)							
Experimental		WB97XD/ (6-31G +(p.d)	WB97XD/ (lanl2dz)	B3PW91/ (6-31G+(p.d)	B3PW91/ (lanl2dz)	Minimum Deviation	Maximum Deviation
C21-N21-C211	119.8(4)	130.6	127.5	129.9	129.0	7.7	10.8
C23-N22-C212	123.9(1)	122.5	128.4	126.0	128.5	1.4	4.6
N21-C21-C22	123.3(1)	129.1	124.2	126.8	123.9	0.6	5.8
N21-C21-C27	111.6(1)	113.5	114.8	113.7	114.3	1.9	3.2
N22 -C23-C25	106.9(1)	106.4	106.9	108.2	106.5	0.4	1.3
N22-C23-C24	110.4(1)	112.2	111.2	111.9	111.2	0.8	1.8
C11-N11-C111	120.3(1)	130.6	127.5	129.9	124.9	4.6	10.3
C13-N12-C112	121.1(1)	122.5	128.4	126.0	128.5	1.4	7.4
N21-C211-C212	123.8(1)	129.1	129.7	129.8	129.6	5.3	5.8
N21-C211-C216	117.1(1)	112.9	112.5	112.6	112.5	4.2	4.6
N22-C212-C211	121.5(1)	123.4	126.1	124.8	125.5	1.9	4.6
N22-C212-C213	119.8(1)	118.0	116.1	116.9	116.4	1.8	3.7
N12-C13-C14	110.4(1)	112.2	111.2	111.9	111.2	0.8	1.8
N12-C13-C15	107.9(1)	106.4	106.9	106.2	106.5	1.0	1.7
N11-C111-C112	123.0(1)	129.1	129.3	129.8	124.9	1.9	6.8
N11-C111-C116	117.9(1)	112.9	112.9	112.6	120.7	2.8	5.3
N12-C112-C113	121.1(1)	118.0	116.1	116.9	116.4	3.1	5.0
N12-C112-C111	120.7(1)	123.4	126.1	124.8	125.5	2.7	5.4

The bond angles of N21-C211-C212, N21-C211-C216, N22-C212-C211 and N22-C212-C213 were experimentally determined as 123.8(1), 117.1(1), 121.5(1) and 119.8(1)°, whilst the computed values gave deviations of between 1.8 and 5.8° from the experimental values. The bond angles of N12-C13-C14, N12-C13-C15, N11-C111-C112 and N11-C111-C116 were experimentally determined as 110.4(1), 107.9(1), 123.0(1) and 117.9(1)° with deviations between 0.8 and 6.8° for the computed values. These differences can be attributed to the fact that the experimental results were obtained in the gas phase whilst the computed data were obtained in the gas phase. Also, the different approximations used in the different functionals and basis sets are fundamental to these differences (Hargittai & Hargittai, 1992).

3.3 Summary of reasons for differences in bond parameters

The experimental single C-N bonds ranged between 1.394 to 1.472 Å. The wide difference is attributable to the lack of planarity in the azepine structure. This is seen in the computed results with WB97XD/6-31G+(p,d), WB97XD/(lanl2dz), B3PW91/(6-31G+(p,d) and B3PW91/(lanl2dz) which gave values ranging from 1.3810 to 1.464 Å for the single C-N bond. The use of the hybrid function

which includes long-range correction is helpful in the computation of the azepine structure due to the spatial arrangement of its atoms.

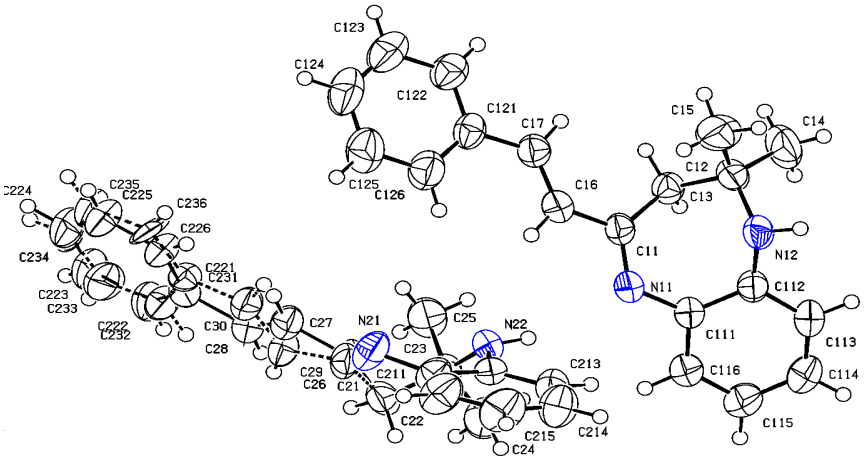

Figure 1 An ORTEP view of (*E*)-2,2-dimethyl-4-styryl-2,3-dihydro-1H-benzo[b][1,4] diazepine showing 50% probability displacement ellipsoids and atom labelling.

The packing showed that there are 8 molecules in the unit cell (**Figure 2**) with the phenyl ring of one of the compounds being disordered. The disordering allows for effective pi-pi interactions which are helpful in stabilizing the molecules in the unit cell.

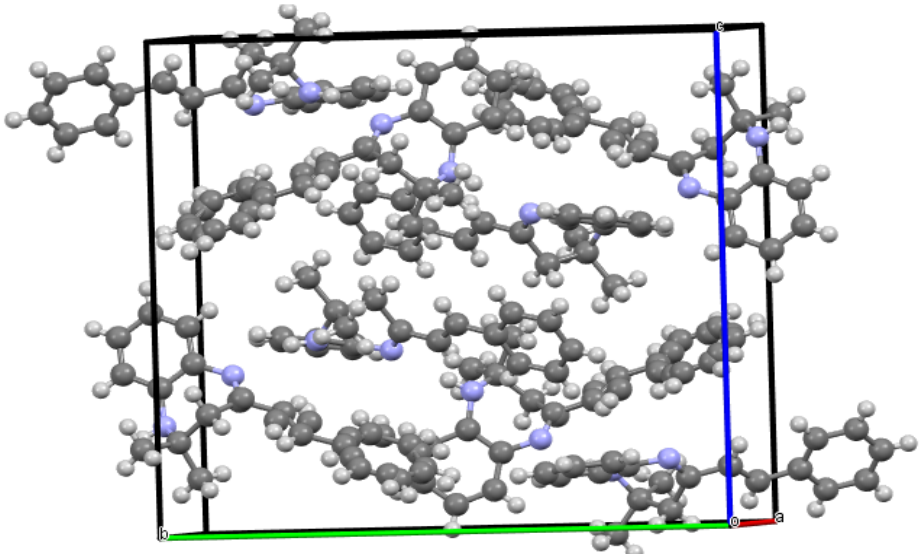

Figure 2 Packing of the molecules of (*E*)-2,2-dimethyl-4-styryl-2,3-dihydro-1H-benzo[b][1,4] diazepine in a unit cell.

3.4 Hirshfeld surface analysis

Hirshfeld surface analysis is a useful tool for visualizing interactions in molecular crystals. CrystalExplorer27 is a computer package that utilizes calculated Hirshfeld surfaces of molecules within a crystal structure to determine the intermolecular interactions between particular molecules or for the crystal structure in its entirety. Hirshfeld surface analysis is a quantitative way to study the intermolecular interactions of the molecules in a crystal structure. Moreover, it gives details of their crystal packing behavior. Hirshfeld surfaces and fingerprint plots were mapped with Crystal Explorer 3.1 software (Wolff *et al*, 2012). The analysis was visualized by the normalized contact distance (*dnorm*), which was obtained using a high surface resolution with a static color scale and computed with the following Eq 1;

$$dnorm = \frac{di - r_i^{vdw}}{r_i^{vdw}} + \frac{de - r_e^{vdw}}{r_e^{vdw}} \qquad \text{Eq1}$$

Where *de* is the distance from the Hirshfeld surface to the nearest nucleus outside the surface, *di* is the corresponding distance to the nearest nucleus inside the surface, and rvdw is the van der Waals radius of the atom (Eltayeb *et al*, 2020). The *dnorm* parameter exhibits a surface with a red-white blue color scheme (Spackman & Jayatilaka, 2009). Bright red spots show the intermolecular contacts less than their vdW radii, while the blue spots show intermolecular contacts longer than their vdW radii. White spots are the sum of their vdW radii. Molecular Hirshfield surfaces comprising of dnorm surface, shape index and curvedness of the compound were generated using a standard (high) surface resolution and is illustrated in **Figure 3**. The dnorm surface was mapped on over the range of -0.3083 Å to 1.5060 Å, shape index in the range of -1.0000 Å. to 1.0000 Å and curvature in the range of -4.0000 Å to 0.4000 Å. **Figure 4** gives the two-dimensional (2D) fingerprint plots from Hirshfeld surface analyses of the compound.

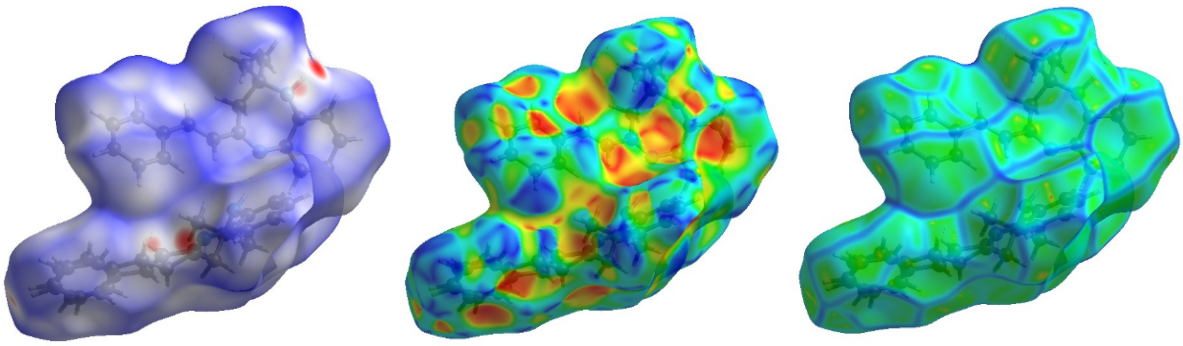

(a) **(b)** **(c)**

Figure 3 Hirshfeld surfaces mapped for (a) d norm surfaces, (b) shape index and (c) curvature of (*E*)-2,2-dimethyl-4-styryl-2,3-dihydro-1H-benzo[b][1,4] diazepine (**1**)

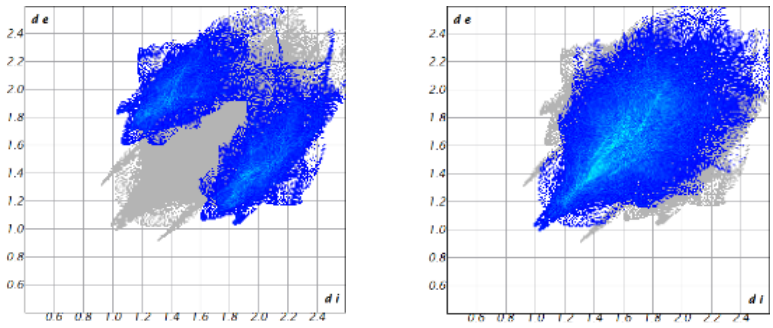

H···C/C···H (31.1%) **H···H /H···H (64.9%)**

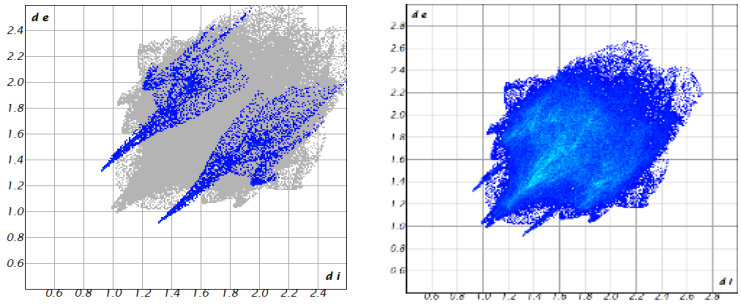

H···N/N···H (3.9%) **All-All (100%)**

Figure 4 Relative contributions to the percentage of Hirshfeld surface area for the various intermolecular contacts in compound **1.**

The H-H interaction gave a contribution of 64.9% to the overall crystal packing, and the C-H (31.1%) and N-H (3.9%) fingerprint plots also provide information about the intermolecular hydrogen bonds and the contribution of the individual elements towards the crystal packing. The shape index mapping (C-Hp interaction) contributed 31.1% of the 2D fingerprint plot. The curvedness shows the electron density of surface curves around the molecular interactions. The flat areas of the surface correspond to low values of curvedness, while the sharp curvature area corresponds to high values of curvedness and usually tends to divide the surface into patches, indicating contacts between neighbouring molecules.

3.5 HOMO–LUMO analysis

The HOMO and LUMO can help in predicting the chemical stability of chemical species (Sarala et al. 2021, Choudhary *et al*, 2019) the LUMO describes the ability to accept an electron whilst the HOMO describes the ability to donate an electron. The energy of the HOMO determines the ionization potential whilst the energy of the LUMO defines the electron affinity. The HOMO and LUMO gap which is the energy difference determines the stability or reactivity of molecules (Matunová *et al*, 2019) and it determines the electrical conductivity of the compound (Padmaja *et al*, 2009). A lower energy gap leads to higher conductivity and vice versa. The hardness of a molecule also corresponds to the gap between the HOMO and LUMO orbitals (Poiyamozhi *et al*, 2012). Chemical reactivity and kinetic stability of the molecule can be characterized using the energy gap (Udhayakala, *et al* 2011). The energies of frontier molecular orbitals, energy band gap (E_{HOMO}-E_{LUMO}), electronegativity (χ), chemical potential (μ), global hardness (η), global softness (S) and global electrophilicity index (ω) all contribute to the reactivity of the molecule concerned. Hardness have been reported to be related to the kinetic stability (Govindarajan *et al*, 2012). The electrophilicity index gives a measure of energy lowering due to highest electron transfer between donor and acceptor (Parr & Chattaraj, 1991, Parr *et al*, 1999, Parthasarathi, *et al* 2003, Parthasarathi et al, 2004). Electrophilicity is a descriptor of reactivity that allows a quantitative classification of the global electrophilic nature of a molecule within a relative scale. The HOMO–LUMO energy levels of the compound determined using WB97XD/(6-31G+(p,d), WB97XD/(lanl2dz), B3PW91/(6-31G+(p,d) and B3PW91/(lanl2dz) levels of theory and basis set are provided in **Table S1**. The HOMO and LUMO for the compound gave energy gaps of between 0.12117 and 0.25915 eV.

3.6 Computed ^{1}H NMR

The Wb97xd/6-311G (2d,2p)/CPCM (DMSO) level (Oliveira *et al*, 2021) was used for the optimization and computation of ^{1}H NMR for each of the optimized structures. The calculated HNMR shifts were affected by the variation in geometry as shown in **Figures 5,** and the results were plotted using multiwfn (Lu & Chen, 2012). The greatest variation in the prediction of the chemical shifts was GIAO calculations for the diazepine ring and the alkene functionality as a further indication of the variation in geometry at the WB97XD/ (6-31G+(p,d), WB97XD/(lanl2dz), B3PW91/(6-31G+(p,d) and B3PW91/(lanl2dz) levels.

The ANMR software (ANMR Ver. 3.5) (Grimme, *et al*, 2017) together with ORCA (Neese, *et al*, 2020) software was used to obtain more representative and more accurate chemical shifts. Pbe0[SMD]/def2-TZVP//pbeh-3c[SMD]/def2-mSVP level (with DMSO as solvent) was used for the calculation. **Figure 6** show the predicted vs experimental ^{1}H NMR spectra for (*E*)-2,2-dimethyl-4-styryl-2,3-dihydro-1H-benzo[b][1,4] diazepine.

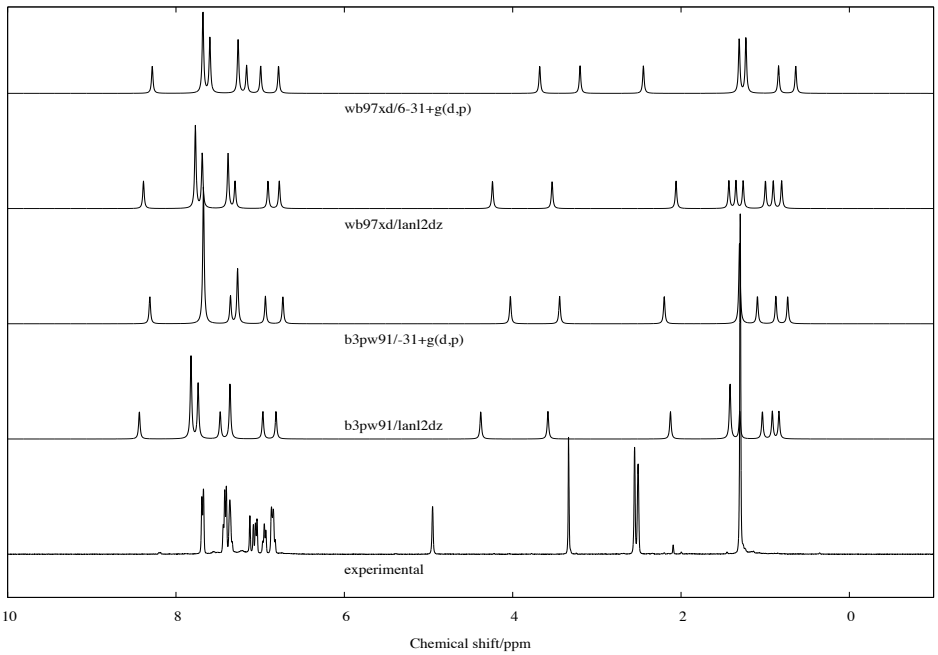

Figure 5 Computed ^{1}H NMR of (E)-2,2-dimethyl-4-styryl-2,3-dihydro-1H-benzo[b][1,4] diazepine using WB97XD/(6-31G+(p,d), WB97XD/(lanl2dz), B3PW91/(6-31G+(p,d) and B3PW91/(lanl2dz) levels

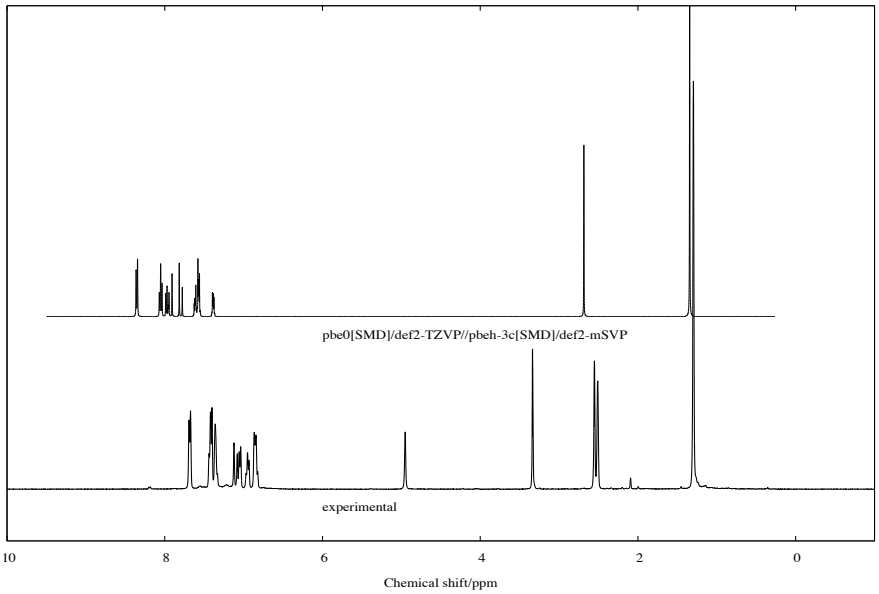

Figure 6 Comparison of computed ^{1}H NMR with experimental results for (*E*)-2,2-dimethyl-4-styryl-2,3-dihydro-1H-benzo[b][1,4] diazepine computed at pbe0[SMD]/def2-TZVP//pbeh-3c[SMD]/def2-mSVP level (with DMSO as solvent). The predicted spectra indicated a mild deshielding of aromatic signals, with coupling constants that matched the experimental data.

3.7 Vibrational frequency

The vibrational data from different computational levels were to obtain the theoretical IR spectra, the plots generated were converted using the irspec.f fortran program (Matzinger & Bally (2000). The frequencies were scaled by a factor of 0.963. The results showed good agreement in the spectra between the different levels of theory, with the greatest variation above 3500 wavenumbers. **Figure 7**, gives the predicted IR spectra with the key bands that are reported in the experimental section indicated for comparison. The computed IR contained all the major functional groups in the experimental data.

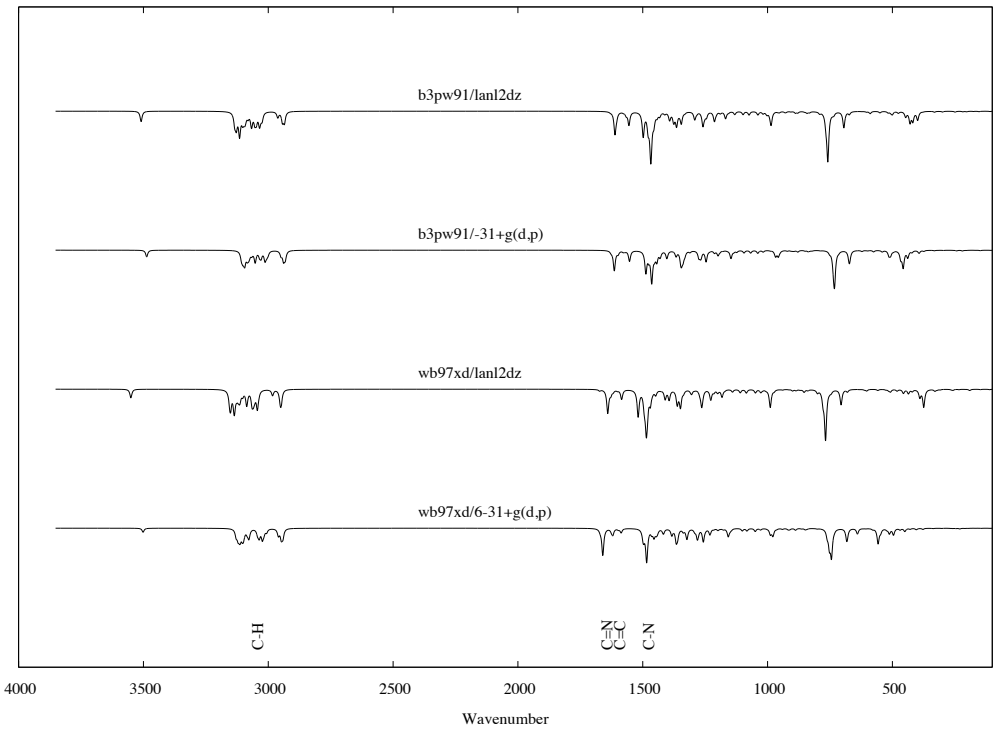

Figure 7 Computed vibrational spectroscopy (IR) of (*E*)-2,2-dimethyl-4-styryl-2,3-dihydro-1H-benzo[b][1,4] diazepine using WB97XD/(6-31G+(p,d), WB97XD/(lanl2dz), B3PW91/(6-31G+(p,d) and B3PW91/(lanl2dz) levels

Conclusion

The single crystal X-ray structure for (*E*)-2,2-dimethyl-4-styryl-2,3-dihydro-1H-benzo[b][1,4] diazepine showed that the compound crystallized in the monoclinic space group *P21/c*, with eight molecules in the unit cell held together Van der Waals interaction. The Hirsfeld surface analysis has been presented to provide quantitative information on the nature and type of intermolecular contacts.

Acknowledgement: We are also grateful for the helpful support of CHPC (www.chpc.ac.za) (CHEM0864)

Disclosure statement: *Conflict of Interest:* The authors declare that there are no conflicts of interest.
Compliance with Ethical Standards: This article does not contain any studies involving human or animal subjects.

References

APEX2 SADABS and SAINT (2010). Bruker AXS Inc: Madison, WI, USA.

Ait Lahcen M., Adardour M., Mortada S., Oubahmane M., Hmaimou S., Loughzail M., Hdoufane I., Lahmidi S., Faouzi M.A, Cherqaoui D., Mague J. T.& Baouid A. (2023) Synthesis, characterization, X-ray, α-glucosidase inhibition and molecular docking study of new triazolic systems based on 1,5-benzodiazepine via 1,3-dipolar cycloaddition reactions, *Journal of Biomolecular Structure and Dynamics*, DOI: 10.1080/07391102.2023.2203263

Bano H., Shafi S., Siddiqui H., Choudhary M. I., Yousuf S. (2017) Synthesis, single crystal X-ray diffraction, Hirshfeld surface and biological activity of quinolone derivatives, *Eur. J. Chem*., 8(4), 422−429. https://doi.org/10.5155/eurjchem.8.4.422-429.1651

Belhassan A., Zaki H., Benlyas M., Lakhlifi T., Bouachrine M. (2019) Study of novel triazolo-benzodiazepine analogues as antidepressants targeting by molecular docking and ADMET properties prediction. *Heliyon* 5, e02446. https://doi.org/10.1016/j.heliyon.2019.e02446

Bronisz K., Ostafin M., Kh. Poleshchuk O., Mielcarek J., Nogaj B. (2006) Studies of the electronic structure and biological activity of chosen 1,4-benzodiazepines by 35Cl NQR spectroscopy and DFT calculations, *Chem. Phys.*, 330, 301–306. DOI:10.1016/j.chemphys.2006.09.001

Choudhary V., Bhatt A., Dash D., Sharma N. (2019) DFT calculations on molecular structures, HOMO–LUMO study, reactivity descriptors and spectral analyses of newly synthesized diorganotin (IV) 2-chloridophenylacetohydroxamate complexes. *J. Comput Chem*., 40(27), 2354−2363. https://doi.org/10.1002/jcc.26012

Eltayeb N. E., Şen F., Lasri J., Hussien M. A., Elsilk S. E., Babgi B.A., Gökce H., Sert Y. (2020). Hirshfeld Surface analysis, spectroscopic, biological studies and molecular docking of (4E)-4-((naphthalen-2-yl)methyleneamino)-1,2-dihydro-2,3-dimethyl-1-phenylpyrazol-5-one. J. Mol. Struc., 1202, 127315. https://doi.org/10.1016/j.molstruc.2019.127315

Elangovan N., Thomas R., Sowrirajan S. (2022) Synthesis of Schiff base (E)-4-((2-hydroxy-3,5-diiodobenzylidene)amino)-N-thiazole-2-yl)benzenesulfonamide with antimicrobial potential, structural features, experimental biological screening and quantum mechanical studies, *J Mol Struc.,* 1250 (1), 131762. https://doi.org/10.1016/j.molstruc.2021.131762

Faidallah H. M., Taib L. A., Albeladi S. N. A., Ur Rahman M. E., Ali F., Zahrani A. I., Arshad M. N., Asiri A. M. (2015) Synthesis, crystal structures and cytotoxic activity of new 1,3,4,5-tetrahydro2H-1,5-benzodiazepine derivatives *J. Chem. Res*., 39, 502–508. Doi: 10.3184/174751915X14396478950860

Flores-Hidalgo, M. A., Barraza-Jiménez. D., Glossman-Mitnik D. (2011) Effects of sulfur substitutional impurities on (ZnO)n clusters (n = 4–12) using density functional theory *Comp. & Theo. Chem*., 965, 154–162 https://doi.org/10.1016/j.comptc.2011.01.037

El Assyry A., Benali B., Lakhrissi B. (2013) Effect of the methyl group on intermolecular characteristics of benzodiazepine-2,4-dione, *Mor J chem.,* 1, 1-10, https://doi.org/10.48317/IMIST.PRSM/morjchem-v1i1.1851

El Ghayati L., Sert Y., Sebbar N. K., Ramli Y., Ahabchane N. H., Talbaoui A., Mague J. T., El Ibrahimi B., Taha M. L., Essassi E. I. M., Al-Zaqri N., Alsalme A. (2021) Syntheses of novel 1,5-benzodiazepine derivatives: Crystal structures, spectroscopic characterizations, Hirshfeld surface analyses, molecular docking studies, DFT calculations, corrosion inhibition anticipation, and antibacterial activities J Heterocycl. Chem., 58(1), 270−289 https://doi.org/10.1002/jhet.4167.

Grimme S., Bannwarth C., Dohm S., Hansen A., Pisarek J., Pracht P., Seibert J., Neese F. (2017) Fully Automated Quantum-Chemistry-Based Computation of Spin-Spin-Coupled Nuclear Magnetic Resonance Spectra Angew. Chem. Int. Ed. 56, 14763−14769 doi: 10.1002/anie.201708266.

Gomes L.R., Neves L.M., Santos B.F., Beleza J., Lowd J.N. (2011) Structural and electronic effects of the C2' substituent in 1,4–benzodiazepines *Eur. J. Chem*., 2(1), 1−7 DOI: 10.5155/eurjchem.2.1.1-7.322

Govindarajan M., Periandy S., Carthigayen. K. (2012) FT-IR and FT-Raman spectra, thermo dynamical behavior, HOMO and LUMO, UV, NLO properties, computed frequency estimation analysis and electronic structure calculations on α-bromotoluene *Spectrochim. Acta A* 97, 411– 422 https://doi.org/10.1016/j.saa.2012.06.028

Hargittai M., Hargittai I. Experimental and computed bond lengths: The importance of their differences (1992) *Int J. Quantum Chem*., 44 (6), 1057-1067 https://doi.org/10.1002/qua.560440610

Hamdane F., Lechauve C., Marden M. C., Golinelli-Pimpaneau B. (2009) Pseudo-merohedral twinning in monoclinic crystals of wild-type human brain neuroglobin *Acta Cryst. D*., *65*, 388–392 DOI:10.1107/S0907444909003382

Hubschle C. B., Sheldrick G. M., Dittrich B. (2011) ShelXle: a Qt graphical user interface for SHELXL *J. Appl. Cryst*., 44, 1281 https://doi.org/10.1107/S0021889811043202.

Koubi Y., Hajji H., Moukhliss Y., El Khatabi K., El Masaoudy Y., Maghat H., Ajana A., Bouachrine M., Lakhlifi T. (2022). in silico studies of 1,4-disubstituted 1,2,3-triazole with amide functionality antimicrobial evaluation against Escherichia coli using 3D-QSAR, molecular docking, and ADMET properties, *Mor. J. Chem.*, 10, 689-702, https://doi.org/10.48317/IMIST.PRSM/morjchem-v10i4.34292

Kositsyn Y.M.; de Abreu M.S.; Kolesnikova T.O.; Lagunin A.A.; Poroikov V.V.; Harutyunyan H.S.; Yenkoyan K.B.; Kalueff A.V. (2023) Towards Novel Potential Molecular Targets for Antidepressant and Antipsychotic Pharmacotherapies. *Int. J. Mol. Sci.*, 24, 9482. doi.org/10.3390/ijms24119482

Lu T., Chen F. (2012) Multiwfn: A Multifunctional Wavefunction Analyzer. *J. Comput. Chem*., 33, 580−592 https://doi.org/10.1002/jcc.22885.

Matunová P., Jirásek V., Rezek B. (2019) DFT calculations reveal pronounced HOMO–LUMO spatial separation in polypyrrole–nanodiamond systems *Phys. Chem. Chem*., 21, 11033−11042 https://doi.org/10.1039/C8CP07622G.

Matzinger S., Bally T. (2000) Spectroscopic Characterization of Matrix-Isolated Phenylcarbene and

Cycloheptatetraene. *J. Phys. Chem*., A 104, 3544−3552 https://doi.org/10.1021/jp993496j.
Neese F., Wennmohs F., Becker U., Riplinger C. (2020) The ORCA quantum chemistry program package *J. Chem. Phys*., 152, 224108 https://doi.org/10.1063/5.0004608.
Odame F., Schoeman R., Krause J., Hosten E. C., Tshentu Z. R., Frost C. L. (2021) Synthesis, characterization, crystal structures, and anticancer activity of some new 2,3-dihydro-1,5-benzoxazepines *Med. Chem. Res.*, *30*, 987–1004. https://doi.org/10.1007/s00044-021-02706-9
Odame F., Hosten E. C., Betz R., Krause J., Frost C. L., Lobb K., Tshentu. Z. R. (2021) Synthesis, characterization, computational studies and DPPH scavenging activity of some triazatetracyclic derivatives *J. Iranian Chem. Soc*., 18, 1979–1995. https://doi.org/10.1007/s13738-021-02158-3
Odame F., Kleyi P., Hosten E. C., Betz R., Lobb K., Tshentu Z. R. (2013) The Formation of 2,2,4-Trimethyl-2,3-dihydro-1H-1,5-Benzodiazepine from 1,2-Diaminobenzene in the Presence of Acetone *Molecules* 18, 14293–14305 https://doi.org/10.3390/molecules181114293.
de Oliveira M. T., Alves J. M. A., Braga A. A. C., Wilson D. J. D., Barboza C. A. (2021) Do Double-Hybrid Exchange-Correlation Functionals Provide Accurate Chemical Shifts? A Benchmark Assessment for Proton NMR *J. Chem. Theory Comput*., 17(11), 6876–6885 doi:10.1021/acs.jctc.1c00604.
Padmaja L., Kunar R. C., Sajan D., Joe I. H., Jayakunmar V. S., Pettit G. R., Nielsen O. F. (2009) Density functional study on the structural conformations and intramolecular charge transfer from the vibrational spectra of the anticancer drug combretastatin-A2 *J. Raman Spectrosc*., 40, 419–428 https://doi.org/10.1002/jrs.2145
Parr R.G., Chattaraj P. K. (1991) Principle of maximum hardness *J. Am. Chem. Soc*., 113, 1854–1855 https://doi.org/10.1021/ja00005a072.
Parr R. G., Szentpaly L. V., Liu S., (1999) Electrophilicity Index *J. Am. Chem. Soc*., 121, 1922–1924 https://doi.org/10.1021/ja983494x.
Parthasarathi R., Padmanabhan J., Subramanian V., Maiti B., Chattaraj P. K. (2003) Chemical Reactivity Profiles of Two Selected Polychlorinated Biphenyls *J. Phys*. *Chem*. A, 107, (48) 10346–10352. https://doi.org/10.1021/jp035620b
Parthasarathi R., Padmanabhan J., Subramanian V., Maiti B., Chattaraj P. K. (2004) Toxicity analysis of 33'44'5-pentachloro biphenyl through chemical reactivity and selectivity profiles *Curr. Sci*., 2004, 86, 535–542 https://www.jstor.org/stable/24107906.
Poiyamozhi A., Sundaraganesan N., Karabacak M., Tanrıverdi O., Kurt M. (2012) The spectroscopic (FTIR, FT-Raman, UV and NMR), first-order hyperpolarizability and HOMO–LUMO analysis of 4-amino-5-chloro-2-methoxybenzoic acid *J. Mol. Struc* 1024, 1–12. doi.org/10.1016/j.molstruc.2012.05.008
Sheldrick G. M. (2008) A Short History of SHELX. *Acta. Cryst A*. 64, 112, doi:10.1107/S0108767307043930
Safna Hussan K. P., Thayyil M. S., Rajan V. K., Muraleedharan K. (2019) DFT studies on global parameters, antioxidant mechanism and molecular docking of amlodipine besylate, *Comput. Biol. Chem*., 80, 46−53. https://doi.org/10.1016/j.compbiolchem.2019.03.006
Sarala S., Geetha S. K., Muthu S., Irfan A. (2021) Computational investigation, comparative approaches, molecular structural, vibrational spectral, non-covalent interaction (NCI), and electron excitations analysis of benzodiazepine derivatives *J. Mol. Model*. 27, 266 doi: 10.1007/s00894-021-04877-z.
Sevvanthi S., Muthua S., Aayisha S., Rameshe P., Raja. M. (2020) Spectroscopic (FT-IR, FT-Raman and UV-Vis), computational (ELF, LOL, NBO, HOMO-LUMO, Fukui, MEP) studies and molecular docking on benzodiazepine derivatives-heterocyclic organic arenes, *Chem. Data Collect.,* 30, 100574 https://doi.org/10.1016/j.cdc.2020.100574.
Selvaraju K., Kumaradhas P. (2015) Charge Density Analysis and Transport Properties of TTF Based Molecular Nanowires: A DFT Approach, *J. Nanosci*., Article ID806181. doi.org/10.1155/2015/806181
Shaik A. B., Bhandare R. R., Nissankararao S., Lokesh B. V. S., Shahanaaz S., Rahman M. M. (2021) Synthesis, and biological screening of chloropyrazine conjugated benzothiazepine derivatives as potential antimicrobial, antitubercular and cytotoxic agents *Arab. J. Chem*., 14(2), 102915, 1–15 https://doi.org/10.1016/j.arabjc.2020.10291
Spackman M. A., Jayatilaka D. (2009) Hirshfeld surface analysis *CrystEngComm*.,*11(1)*,19–32. https://doi.org/10.1039/B818330A
Tabti K., El Mchichi L., Moukhliss Y., Singh G., Sbai A., maghat H., bouachrine M., Lakhlifi T. (2022). CoMFA Topomer, CoMFA, CoMSIA, HQSAR, docking molecular, dynamique study and ADMET study on phenyloxylpropyl isoxazole derivatives for coxsackie virus B3 virus inhibitors activity, *Mor. J. Chem.,* 10, 703-725, https://doi.org/10.48317/IMIST.PRSM/morjchem-v10i4.34319

Taha N. I. (2017) Synthesis of 1,3-Oxazepine Derivatives Derived from 2-(1H-Benzo[d][1,2,3]Triazol-1-yl)Acetohydrazide by Using Microwave Irradiation *Int. J. Org. Chem*., 7(7), 219–228 DOI:10.4236/ijoc.2017.73016

Udhayakala P., Jayanthi A., Rajendiran T. V., Gunasekaran S. (2011) Molecular structure, FT-IR and FT-Raman spectra and HOMOLUMO analysis of 2-methoxy-4-nitroaniline using ab initio HF and DFT (B3LYP/B3PW91) calculations *Arch. Appl. Sci. Res*., 3(4), 424–439. DOI:10.1002/jrs.2145

Wolff S. K., Grimwood D.J., McKinnon J. J., Turner M. J., Jayatilaka D., Spackman M. A. (2012) Perth